catalysts

MDPI

Article

Ru- and Rh-Based Catalysts for CO_2 Methanation Assisted by Non-Thermal Plasma

Eugenio Meloni *, Liberato Cafiero, Simona Renda, Marco Martino, Mariaconcetta Pierro and Vincenzo Palma

Department of Industrial Engineering, University of Salerno, 84084 Fisciano, Italy
* Correspondence: emeloni@unisa.it

Abstract: The need to reduce the concentration of CO_2 in the atmosphere is becoming increasingly necessary since it is considered the main factor responsible for climate change. Carbon Capture and Utilization (CCU) technology offers the opportunity to obtain a wide range of chemicals using this molecule as a raw material. In this work, the catalytic Non-Thermal Plasma (NTP)-assisted hydrogenation of CO_2 to CH_4 (methanation reaction) in a Dielectric Barrier Discharge (DBD) reactor was investigated. Four different Ru- and Rh-based catalysts were prepared starting from γ-Al_2O_3 spheres, characterized and tested in both thermal and NTP-assisted methanation under different operating conditions. The experimental tests evidenced the very positive effect of the NTP application on the catalytic performance, highlighting that for all the catalysts the same CO_2 conversion was reached at a temperature 150 °C lower with respect to the conventional thermal reaction. Among the prepared catalysts, the bimetallic ones showed the best performance, reaching a CO_2 conversion of 97% at about 180 °C with a lower energy consumption with respect to similar catalysts present in the literature.

Keywords: non-thermal plasma; methanation; sustainability; electrification

check for updates

Citation: Meloni, E.; Cafiero, L.; Renda, S.; Martino, M.; Pierro, M.; Palma, V. Ru- and Rh-Based Catalysts for CO_2 Methanation Assisted by Non-Thermal Plasma. *Catalysts* **2023**, *13*, 488. https://doi.org/10.3390/catal13030488

Academic Editor: Zhixin Yu

Received: 14 February 2023
Revised: 24 February 2023
Accepted: 27 February 2023
Published: 28 February 2023

1. Introduction

Carbon dioxide (CO_2) is a product of many human activities, from daily to industrial ones. The need to reduce its concentration in the atmosphere is becoming increasingly necessary since it is considered the main factor responsible for climate change. In particular, global CO_2 emissions reached their highest level in history in 2021 [1]. This anomalous growth was linked to the high increment in energy demand after the COVID-19 crisis, which, despite the increase of energy from renewable sources, has also lead to a return to coal, which accounted for over 40% of the overall CO_2 emissions in 2021 [2]. In recent years, various sectors have moved towards greener methods, thus limiting their emissions in terms of CO_2. However, this may not be enough to limit global warming and it may also be necessary to combine these methods with systems for CO_2 capture. By geologically confining the captured CO_2, many drawbacks, such as uncontrolled release in the atmosphere, high energy consumption and high costs, may occur [3]. Carbon Capture and Utilization (CCU) technology, besides reducing the CO_2 concentrations in the atmosphere, also offers the opportunity to obtain a wide range of chemicals using this molecule as a raw material [4,5]. Recently, another novel technology, the Power-to-Gas (PtG) approach, has begun development for the generation of hydrogen fuel from excess electricity from renewable sources [6]. Since the storage and use of hydrogen require expensive infrastructure, converting it into methane can represent a better solution. Therefore, a combination of the two aforementioned technologies, CCU and PtG, may result in the "Power-to-Methane" process, obtaining "green" methane through the Sabatier reaction (Equation (1)).

$$CO_2 + 4H_2 \leftrightarrows CH_4 + H_2O \rightarrow (\Delta H^0{}_{298k} = -165.12 kJ/mol) \quad (1)$$

The conventional methanation process is usually carried out in the temperature range 300–500 °C, and under these reaction conditions several side reactions may occur. The need for a high temperature is also linked to the strong stability of the C–O bond, which makes the activation of the CO_2 molecule challenging for any catalyst. The most used catalysts for CO_2 methanation are the Ni-based ones due to their good catalytic performance, as well as their cheapness and availability. The amount of Ni in the catalytic formulation is usually within the range 10–20%wt, which is deposited on a support with high porous volume and a good surface area for obtaining a good dispersion. According to recent works [7–9], the best supports for Ni-based catalysts are ZrO_2 and CeO_2 because, compared to Al_2O_3, TiO_2 and SiO_2, they have a larger number of oxygen vacancies which can enable great amounts of CO_2 adsorption and therefore make CO_2 activation easier. Additionally, noble metals, such as ruthenium and rhodium, are very active and selective in the CO_2 methanation process, thanks to their low activation temperature and their high reducibility and stability. In this case, the amount of noble metal deposited on the support is particularly important, both from a catalytic and an economic point of view since noble metals are expensive. In several studies, Ru-based catalysts have shown a good catalytic activity and selectivity to CH_4 if the metal is loaded in the range 0.5–4%wt [10–13]. This low amount of Ru makes these catalysts very promising for a potential industrial CO_2 methanation application. Additionally, Rh-based catalysts, by using a small amount of metal in the catalytic formulation, are active and selective in the methanation process. In particular, their catalytic activity and selectivity mainly depend on the OSC (Oxygen Storage Capacity) of the support and on Rh particle sizes; CO_2 methanation efficiency is favoured on smaller Rh particles when dispersed on supports with a lack of oxygen ion lability, and vice versa on supports with high oxygen ion lability [14–17]. However, besides finding high-performance catalysts, the main challenge of the considered process consists of lowering the operating temperatures and pressures, which cause high operating and investment costs.

Lately, many studies in the literature have focused on the use of non-thermal plasma (NTP) in the methanation processes [18]. Additionally, NTP, known as non-equilibrium plasma, can produce a variety of active species, such as electrons, ions, excited neutrons and low-temperature radicals useful for activating the carbon dioxide molecule at temperatures close to ambient. NTP-assisted catalytic processes are characterized by fast start-up and shutdown and can be carried out at atmospheric pressure and temperature, thus requiring lower energy costs [19]. Moreover, the application of plasma in catalytic systems generates several advantages, as this activates the gas molecules and modifies the surface of the catalyst, generating new active sites for adsorption and, in this way, creating new reaction paths [20]. In particular, the combination of NTP and catalysis can significantly enhance CO_2 conversion and CH_4 selectivity, respectively, from values lower than 15% up to values around 70% for both parameters [21]. Most of the studies have focused on Dielectric Barrier Discharge (DBD)-type plasma; in these studies, the applied voltage varied in the range 7–20 kV, with a power ranging from 3 to 15 W [22,23]. From a comparison between conventional and NTP-assisted methanation, Biset-Peiró et al. [24] found that the use of NTP allowed the same results of conversion and selectivity, but at lower temperatures, to be obtained using a Ni/γ-Al_2O_3 catalyst. Additionally, Xu et al. [25] reported that, at the same temperature, CO_2 conversion under NTP conditions is more than six times higher that under the thermal conditions. In plasma-assisted processes, the support has a greater influence on the catalytic performance, as reported by Nizio et al. [26,27]; the use of support with low/medium basicity can lead to enhanced results, since the kinetically relevant step is the adsorption of CO_2 leading to adsorbed CO and adsorbed O. However, by employing noble metals, further particular reaction paths can occur. Xu et al. [28] revealed that the synergy of NTP and Ru species plays a key role in the catalytic activity of CO_2 methanation.

Starting from a study of the literature, in this work, different mono- and bimetallic Ru- and Rh-based catalysts were prepared starting from γ-Al_2O_3 spheres (1–2 mm), also aiming

to investigate the effect of the impregnation order on the catalytic activity. The prepared catalysts were tested both in the conventional thermal and in the NTP-assisted (using a DBD reactor) methanation reactions under two different weight hourly space velocity (WHSV) values. The experimental tests evidenced the very positive effect of the NTP application on the catalytic performance, highlighting that for all the catalysts the same CO_2 conversion was reached at a temperature 100 °C lower compared to the conventional thermal reaction. Among the prepared catalysts, the bimetallic ones showed the best performance, reaching a CO_2 conversion of 97% at about 180 °C with a lower energy consumption with respect to similar catalysts present in the literature.

2. Results and Discussion

2.1. Catalyst Characterization

2.1.1. Physical Characteristics

The results of Hg intrusion porosimetry and N_2 @ 77K physisorption are reported in Figures 1 and 2. as specific pore volume vs. pore size, and total adsorbed volume vs. P/P_0, respectively.

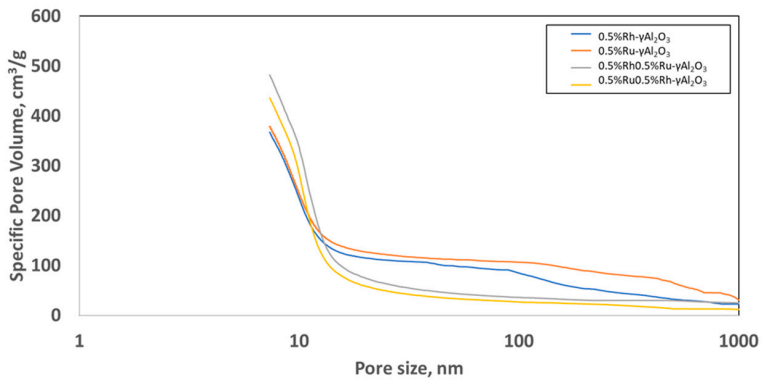

Figure 1. Specific pore volume vs. pore size for the catalytic samples from the Hg intrusion porosimetry.

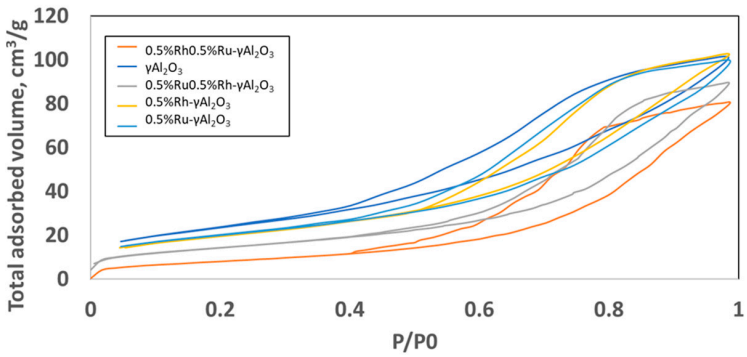

Figure 2. Catalysts' adsorption–desorption isotherms compared with the bare γAl_2O_3 spheres.

As can be seen from Figure 1, and particularly from the increasing slope of the left part of the graph in correspondence with the smaller pore size, there is a considerable portion of the pores which could not be evaluated by the porosimeter; hence, a highly micro- and mesoporous behaviour can be supposed for all the catalysts. This supposition is confirmed by the adsorption–desorption isotherms reported in Figure 2. The isotherms relating to the loaded catalysts were all of type IV and presented a type H3 hysteresis due to the presence of both micropores and mesopores. It is important to note that the addition of the active species reduced the amount of micropores; in fact, the height of the isotherm curve at low values of P/P_0 (left side of the diagram) decreased after Rh and Ru deposition on the support (blue curve), which is particularly visible on the bimetallic catalysts (grey and

orange curves). Nevertheless, it can be stated that all the catalysts kept the mesoporous behaviour of the support.

A summary of all the main characteristics of the catalysts is reported in Table 1:

Table 1. Surface area, pore volume and average pore diameter.

	N_2 @77K Physisorption			Hg Intrusion Porosimetry	
Sample Name	**Surface Area (BET), m^2/g**	**Mesopores Volume, cm^3/g**	**Average Mesopore Diameter, nm**	**Average Pore Diameter, nm**	**Total Pore Volume, cm^3/g**
γ-Al_2O_3	271.000	0.390	4.300	13.600	0.243
Rh-γAl_2O_3	246.000	0.410	4.870	13.860	0.367
Ru-γAl_2O_3	242.000	0.390	5.700	14.400	0.378
RhRu-γAl_2O_3	148.000	0.410	7.410	12.070	0.482
RuRh-γAl_2O_3	232.000	0.460	4.600	11.620	0.436

The Hg intrusion porosimetry showed that the average pore diameter increased with respect to the bare spheres after the deposition of a single active phase, and that the further deposition of the second one led to its decrease. The total pore volume, however, increased with the deposition of the active phases. The Brunauer–Emmett–Teller analysis highlighted a decrease of the catalysts' surface area when compared to the bare support. Furthermore, a sensible increase of the mesopore volume, as well as of the average mesopore diameter, can be noted.

Finally, to better understand the dispersion of the active phases on the support, a SEM-EDX analysis of the catalysts was carried out (Figures 3–6).

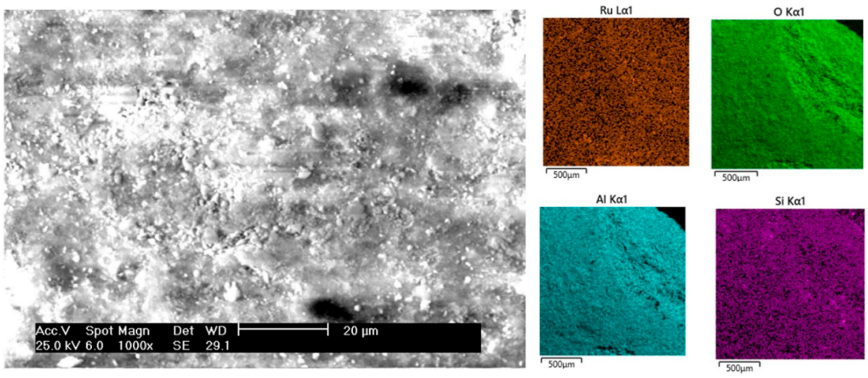

Figure 3. SEM-EDX Ru-γAl_2O_3.

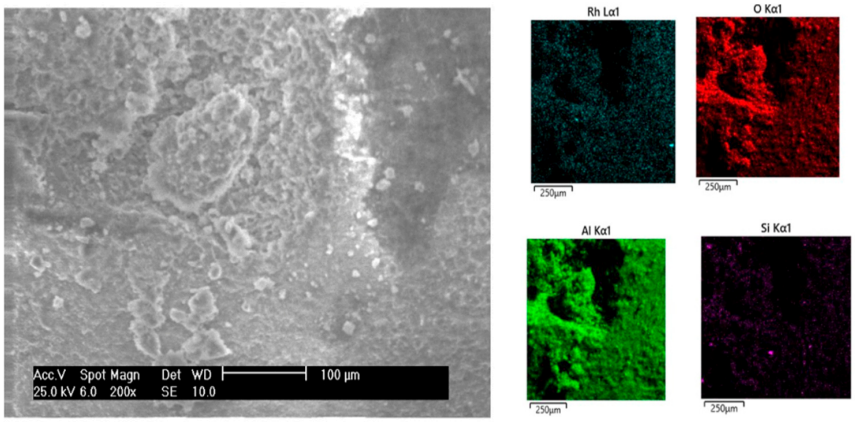

Figure 4. SEM-EDX Rh-γAl_2O_3.

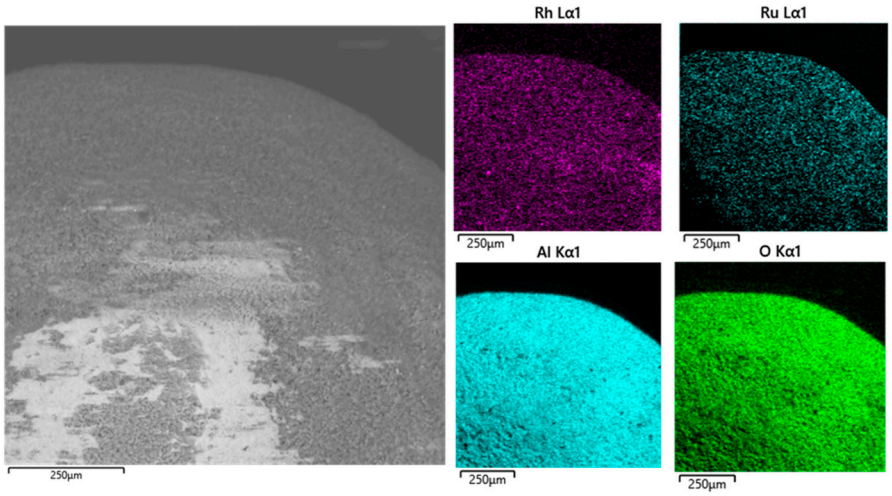

Figure 5. SEM-EDX Ru,Rh-γAl_2O_3.

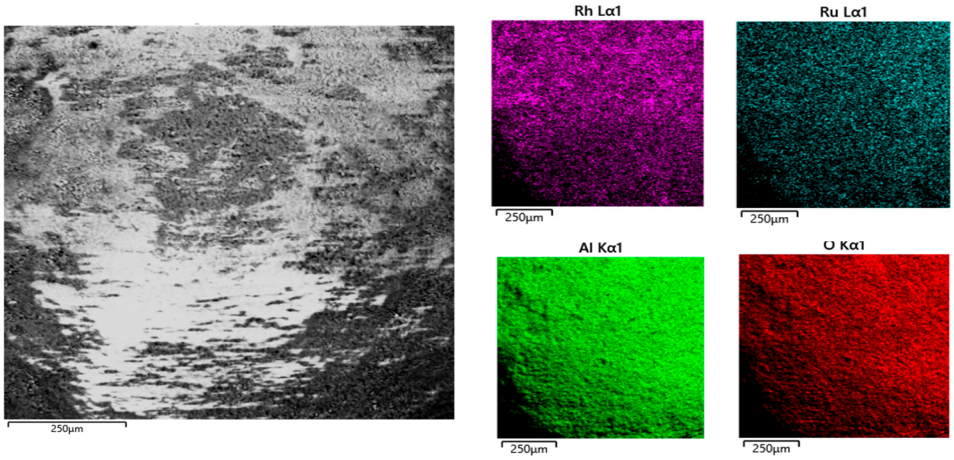

Figure 6. SEM-EDX Rh,Ru-γAl_2O_3.

As can be clearly seen from Figures 3–6, for both the monometallic catalysts and the bimetallic ones, a homogeneous deposition of the active phases on the whole surface of the support was obtained.

2.1.2. Chemical Characteristics

To evaluate the effective loading of the active phases on the support, a H_2-Temperature Programmed Reduction analysis was performed. The results are reported in Figure 7 and in Table 2.

Table 2. Catalysts' theoretical and experimental H_2 consumption.

Catalyst Name	Theorical Hydrogen Uptake, mol	Experimental Hydrogen Uptake, mol
Ru-$\gamma\gamma Al_2O_3$	7.66×10^{-4}	7.40×10^{-4}
Rh-γAl_2O_3	7.64×10^{-4}	7.35×10^{-4}
RhRu-γAl_2O_3	2.70×10^{-3}	2.40×10^{-3}
RuRh-γAl_2O_3	2.70×10^{-3}	2.75×10^{-3}

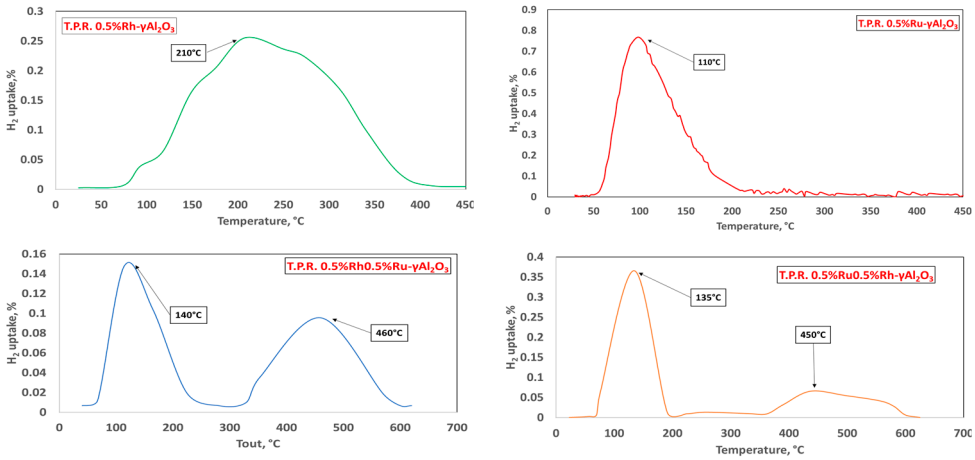

Figure 7. Catalysts' H_2-Temperature Programmed Analysis charts.

From the above reported figure, it can be seen that (i) the monometallic Rh-based catalyst is characterized by the presence of a wide reduction area with two main peaks at 160 and 210 °C, and (ii) the monometallic Ru-based catalyst is characterized by a single peak centred at 110 °C. These results are in good agreement with the literature [29,30]. The bimetallic catalysts are characterized by the presence of two peaks, at lower and higher temperatures, due to a synergic effect of the two metals.

To evaluate the theorical hydrogen consumption for both Ruthenium and Rhodium, the oxides Rh_2O_3 and Ru_2O_3 and the correspondent reduction reactions (Equations (2) and (3)) were considered.

$$Rh_2O_3 + 3H_2 \rightarrow 2Rh + 3H_2O, \quad (2)$$

$$Ru_2O_3 + 3H_2 \rightarrow 2Ru + 3H_2O, \quad (3)$$

As can be seen from Table 2, the theorical and experimental hydrogen consumption are comparable; hence, the active phase loading was verified.

2.2. *Activity Tests*

2.2.1. Thermal Methanation Tests

All four catalysts were tested under the same conditions and the results were evaluated in terms of conversion, selectivity and yield evaluated according to the formulas below:

$$X_{CO_2} = \frac{n^{in}_{CO_2} - n^{out}_{CO_2}}{n^{in}_{CO_2}} \quad (4)$$

$$S_{CH_4} = \frac{n_{CH_4}}{n^{in}_{CO_2} - n^{out}_{CO_2}} \quad (5)$$

$$Y_{CH_4} = \frac{n_{CH_4}}{n^{in}_{CO_2}} \quad (6)$$

in which n_i are the moles of the component "i".

The results relevant to the experimental tests performed at the two WHSV are reported in the following figures (Figures 8 and 9) for all the catalysts.

As can be clearly seen from Figures 8 and 9, the bimetallic catalysts showed the best results both in terms of CO_2 conversion and CH_4 yield in all the investigated temperature ranges. By deeply analysing these figures, one more difference is observable. While for the higher space velocity there was a remarkable difference between all the catalysts' results, with the RuRh-γAl_2O_3 obtaining a CO_2 conversion (which corresponds to the CH_4 yield being the selectivity equal to 1) of about 80% at 320 °C, the results at lower space velocity showed that the bimetallic catalysts had very similar behaviour, with a maximum of 84% in

terms of both CO_2 conversion and CH_4 yield. It is important to highlight that the selectivity followed the pattern of the equilibrium curve at low temperatures and kept high values even at higher temperatures.

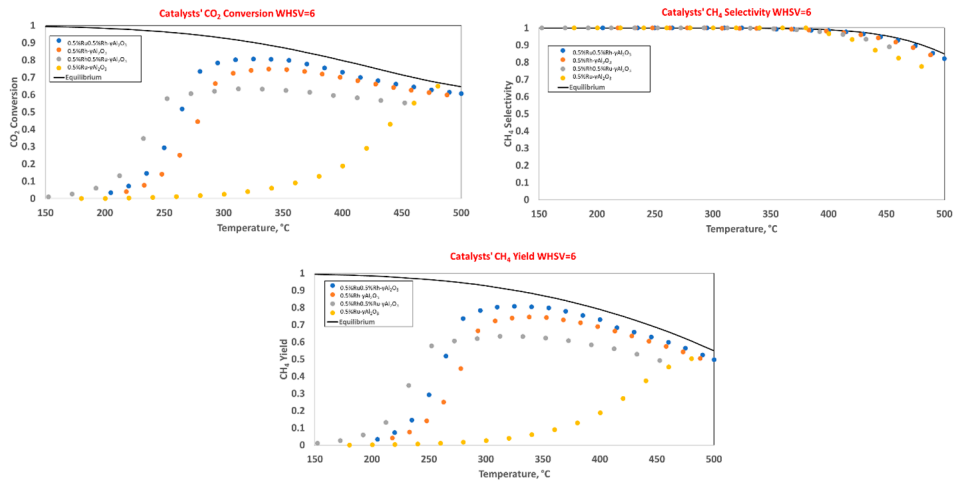

Figure 8. Catalysts' CO_2 conversion, CH_4 selectivity and yield at WHSV = 6 NL/g_{cat}h.

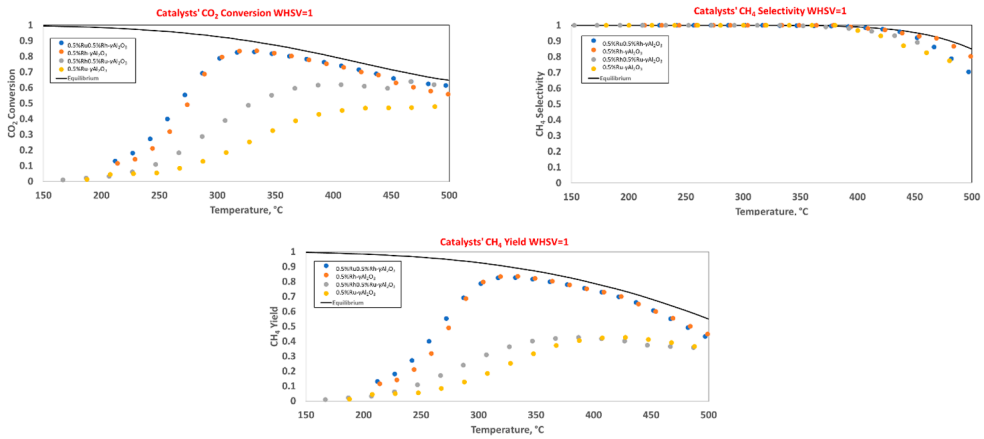

Figure 9. Catalysts' CO_2 conversion, CH_4 selectivity and yield at WHSV = 1 NL/g_{cat}h.

Among the bimetallic catalysts, the RuRh-γAl_2O_3 catalyst was chosen to compare the results obtained at the two space velocities in terms of CH_4 yield (Figure 10).

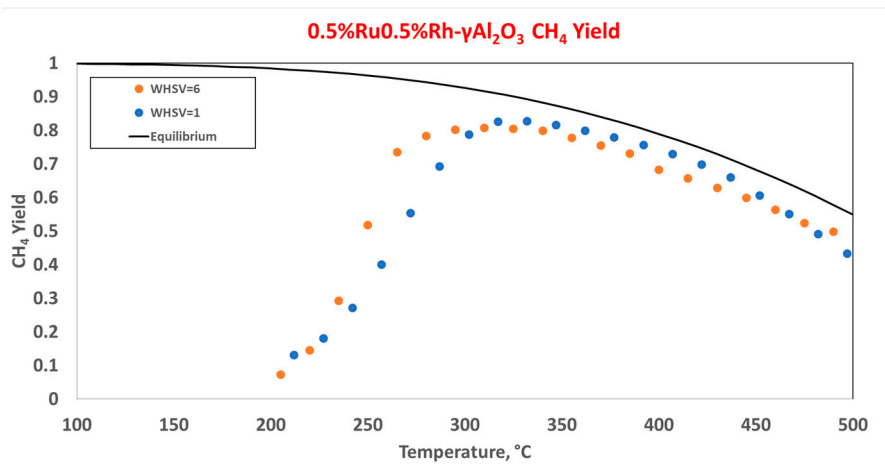

Figure 10. RuRh-γAl_2O_3 CH_4 selectivity comparison between the two space velocities.

Figure 10 shows that tests performed at a higher space velocity (orange curve) obtained the same results at temperatures slightly lower than the lower space velocity one (blue curve), but the latter has a slight increase in terms of CH_4 yield obtaining a maximum CH_4 yield of 84%vol. at 320 °C. However, at higher temperatures it can be seen that the higher space velocity tests produced a higher quantity of CH_4.

2.2.2. Non-Thermal-Plasma-Assisted Methanation Tests

All four catalysts were tested in the NTP-assisted reaction under the same operating conditions of the conventional tests in terms of space velocities. The results are reported in Figure 11 for the higher space velocity.

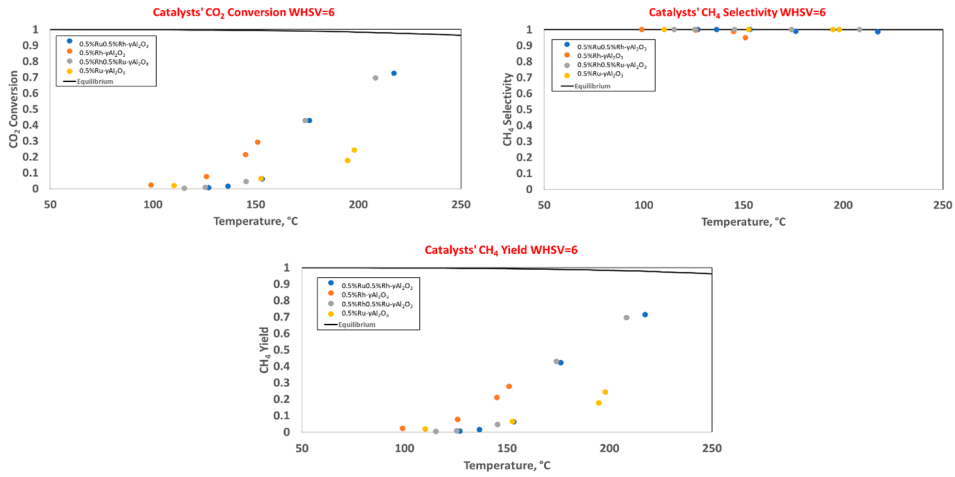

Figure 11. Catalysts' CO_2 conversion, CH_4 selectivity and yield in non-thermal-plasma-assisted tests at WHSV = 6 NL/g_{cat}h.

The data reported above highlighted the very positive effect of the NTP application: the same CO_2 conversion can be obtained at lower temperatures than the thermal process. Moreover, the reported data evidenced, apart from the high selectivity shown by all the catalysts, the best catalytic performance obtained by using the bimetallic catalysts, among which the RuRh-γAl_2O_3 showed the highest CO_2 conversion (about 72%). This result may be ascribable to the high surface area of the latter sample, coupled with the higher mesopore volume and lower pore radius. One more important result is that it was possible to obtain methane starting from 100 °C.

The results relevant to the experimental tests performed at the lower space velocity are reported in Figure 12.

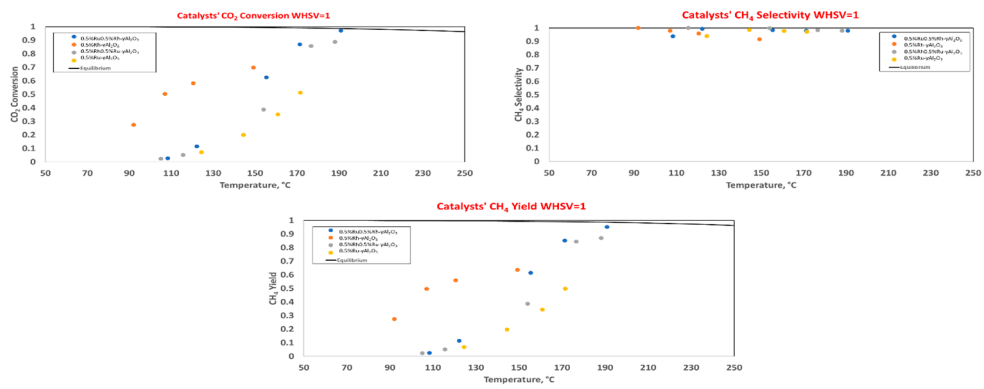

Figure 12. Catalysts' CO_2 conversion, CH_4 selectivity and yield in non-thermal-plasma-assisted tests at WHSV = 1 NL/g_{cat}h.

The most interesting results were obtained in these conditions with bimetallic catalysts. Due to the operating temperature being considerably lower than the thermal process temperature, it was possible to reach CO_2 conversions much higher than the ones obtained in such processes which were limited by the thermodynamic equilibrium. In fact, the best catalyst was RuRh-γAl_2O_3, which approached the equilibrium values at a CO_2 conversion of about 97% at 190 °C, which resulted in a CH_4 yield of 95%.

2.2.3. Thermal/NTP-assisted Methanation Comparison

Finally, to better highlight the importance of the non-thermal-plasma-assisted methanation (Figure 13), a comparison between the best CH_4 yields of RuRh-γAl_2O_3 in both thermal and NTP-assisted tests at the lower space velocity is reported in Figure 6.

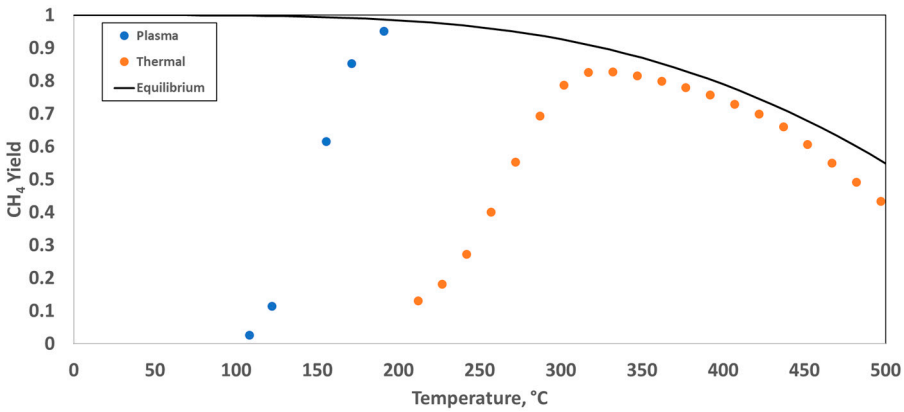

Figure 13. RuRh-γAl_2O_3 CH_4 yield comparison for both thermal and non-thermal-plasma-assisted tests at WHSV = 1 NL/g_{cat}h.

As previously stated, the ability to activate the CO_2 molecules at lower temperatures results in the possibility of reaching yields that would be impossible to reach due to thermodynamic limitations. Furthermore, it is also fundamental to note that it is possible to obtain CH_4 yields similar to the thermal ones at temperatures about 100 °C lower, which would result in a considerably lower energy expense.

2.3. Energy Considerations

It is important to consider the energy consumption of the whole non-thermal plasma assisted process and to compare it with those found in the literature. In order to make a careful comparison, the Specific Energy Input (SEI) index was taken into account and evaluated according to the following formula:

$$Specific\ Energy\ Input\ \left[\frac{kJ}{L}\right] = \frac{P[kW]}{F[L/s]} \quad (7)$$

The results of said comparison are reported in Table 3.

As can be clearly seen from the table above, the specific energy input of the test conducted in the present work is considerably lower than those found in the literature and, when this input is slightly higher those in the literature, the CO_2 conversion and the CH_4 production are considerably higher. Hence, it can be stated that, although the energy efficiency of the present setup is still far from being optimized up to the industrial level, it is a good basis to develop further improvements in the energy efficiency of plasma-catalytic methanation systems.

Table 3. Present work catalysts' SEI, CO_2 conversion and CH_4 production compared with the literature.

Catalyst Name	Operating Conditions	CO_2 Conversion	SEI [kJ/L]	CH_4 Produced [mmol/min]	Reference
0.5%Ru0.5%Rh-γAl_2O_3	Flow rate: 340 mL/min, T = 188.1 °C, H_2:CO_2 = 4; P = 55W	0.97	9.7	14.71	Present work
0.5%Rh0.5%Ru-γAl_2O_3	Flow rate: 340 mL/min, T = 190.1 °C, H_2:CO_2 = 4; P = 55W	0.88	9.7	13.35	Present work
0.5%Ru0.5%Rh-γAl_2O_3	Flow rate: 1 L/min, T = 217.6 °C, H_2:CO_2 = 4; P = 55W	0.73	3.3	32.56	Present work
0.5%Rh0.5%Ru-γAl_2O_3	Flow rate: 1 L/min, T = 208.3 °C, H_2:CO_2 = 4; P = 55W	0.7	3.3	31.23	Present work
15%Ni-$CeZrO_2$	Flow rate: 200 mL/min, T = 170 °C, H_2:CO_2 = 7; P = 16W	0.76	4.8	8.14	[31]
Mn-Al_2O_3	Flow rate: 34.6 mL/min, T = 135 °C, H_2:CO_2 = 4; P = 35W	0.76	60	1.18	[32]
Ni-Al_2O_3	Flow rate: 69.2 mL/min, T = 150 °C, H_2:CO_2 = 4; P = 30W	0.48	26	1.47	[33]
Ru-γAl_2O_3	Flow rate: 80 mL/min, T = 250 °C, H_2:CO_2 = 7; P = 33W	0.18	25	0.14	[34]

3. Materials and Methods

3.1. Preparation of the Catalysts

The catalysts were prepared through the wet impregnation technique. The support, γ-Al_2O_3 in spheres (1–2 mm), was previously calcined at 600 °C and then dipped in a solution of the precursor salts, ruthenium acetylacetonate ($C_{15}H_{21}O_6Ru$) and rhodium nitrate hydrate ($RhN_3O_3 \cdot xH_2O$) for Ru- and Rh-based catalysts, respectively, in acetone for 15 min. After that, the catalysts were dried at 120 °C for 2 h, and finally calcined at 600 °C for 1 h. The bimetallic catalysts differ each other from the order of impregnation of the metals. The metal loading for both mono- and bi-metallic catalysts was of 0.5%wt for each active species.

3.2. Catalysts' Characterization

The prepared samples were characterized by means of physicochemical techniques, such as Hg intrusion porosimetry, Electron Microscopy SEM-EDX and physisorption of N_2 @ 77 K, in order to assess the distribution and dimension of the pores, and to evaluate the distribution of the active phase, both superficial and volumetric. Furthermore, a Temperature-Programmed Reduction (TPR) was carried out to obtain qualitative and quantitative information; thus, the reduced species and the quantity of metal stored on the support. The TPR was conducted with a ramp of 10 °C/min until 500 °C, in presence of 5% H_2 in Ar.

3.3. Experimental Plant

The NTP-assisted tests on the catalysts were carried out in the experimental plant shown in Figure 14. A mass flow controller (MFC) battery was used to feed the gases (Ar, CO_2, H_2) to the quartz reactor, which was linked to the plasma generator through the two electrodes, high voltage and ground. A moisture trap was placed at the exit of the reactor to catch the water produced by the reaction. The composition of the outlet mixture was then analysed by a mass spectrometer. Both composition and temperature data were collected on a computer using specific software.

Two temperature probes were placed inside the reactor, one at the inlet and one at the outlet of the catalytic bed, to detect the temperature trend inside the catalyst. The probes were OPTOCON fibre optic temperature sensors, specifically designed to be inert to electromagnetic fields and in particular to high voltages. The reactor for the NTP-assisted tests was a DBD reactor; this is a quartz tube with an internal chamber where the internal

electrode (high-voltage) is placed, an external metal covering mesh, which is the ground electrode, and between the two electrodes is the dielectric, the catalyst itself. The plasma generator induces the non-equilibrium discharge with an adjustable frequency between 20–60 kHz and a high voltage between 1–40 kV alternative current (AC). The catalytic tests were carried out using a feeding mixture of 48%H_2, 12%CO_2 and 40%Ar, and at two different WHSV, 1 NL/gcat·h and 6 NL/gcat·h, in order to verify if it would have any effect on the catalyst's performance. These conditions were the same for the NTP-assisted and conventional methanation tests. The NTP catalytic tests were carried out by supplying a value of current between 0.1 and 0.6 A, with increments of 0.1 A, and the data were taken once the discharge reached a steady state because this situation also corresponded to a stable value of temperature and composition. Then, the thermal tests were carried out by considering the same temperature values registered for the NTP-assisted process in order to make a comparison between the two process modalities.

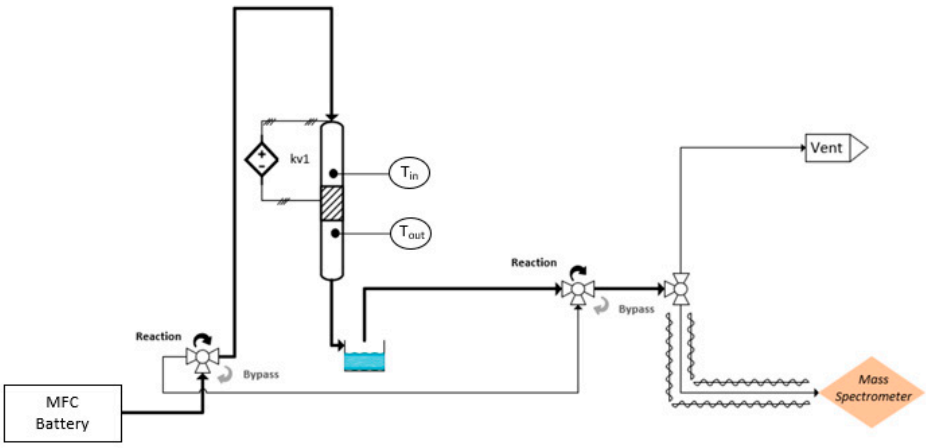

Figure 14. Experimental plant design.

4. Conclusions

In this work, non-thermal-plasma-assisted CO_2 methanation has been studied. Four alumina-supported structured catalysts were prepared, two monometallic ones and two bimetallic ones, the latter prepared by varying the impregnation order of the metals. All the prepared catalysts were characterized and tested in the CO_2 hydrogenation reaction (methanation) both in a thermal plant and in a Dielectric Barrier Reactor (DBD) non-thermal plasma plant. The effect of different parameters (temperature and space velocity), as well as of the impregnation order for the bimetallic catalysts, were studied, and a comparison made between the thermal and the NTP-assisted processes.

A fundamental result of this work is the possibility of obtaining CH_4 yields comparable to the thermal yields at temperatures about 100 °C lower than the latter, granting the possibility of approaching the equilibrium line at higher values. The best catalytic activity (CH_4 yield = 95%vol.) was obtained at 188.1 °C with H_2:CO_2 ratio = 4 by using the catalyst RuRh-γAl_2O_3; the other bimetallic catalyst showed a slightly lower CH_4 yield (88%vol.) at about the same temperature (190 °C). These results were obtained with an SEI (Specific Energy Input) lower than the ones found in the literature by a whole order of magnitude while maintaining higher conversions and yields.

The results shown in this work have demonstrated the possibility of applying the plasma catalysis approach to CO_2 methanation, obtaining remarkable results at temperatures much lower than those of the traditional processes. Possible future improvements may involve the optimization of the reacting system and the study of the catalysts stability over time.

Author Contributions: Conceptualization, E.M., L.C., S.R., M.P., M.M. and V.P.; methodology, E.M., L.C., S.R., M.P., M.M. and V.P.; software, E.M., L.C., S.R., M.P., M.M. and V.P.; validation, E.M., L.C., S.R., M.P., M.M. and V.P.; formal analysis, E.M., L.C., S.R., M.P., M.M. and V.P.; investigation, E.M., L.C., S.R., M.P., M.M. and V.P.; resources, E.M., L.C., S.R., M.P., M.M. and V.P.; data curation, E.M., L.C., S.R., M.P., M.M. and V.P.; writing—original draft preparation, E.M., L.C., S.R., M.P., M.M. and V.P.; writing—review and editing, E.M., L.C., S.R., M.P., M.M. and V.P.; visualization, E.M., L.C., S.R., M.P., M.M. and V.P.; supervision, E.M., L.C., S.R., M.P., M.M. and V.P.; project administration, E.M., L.C., S.R., M.P., M.M. and V.P. All authors have read and agreed to the published version of the manuscript.

Funding: This research received no external funding.

Data Availability Statement: Not applicable.

Acknowledgments: The authors are grateful to Paolo Tramonti for performing the SEM-EDX analysis. The authors are grateful to Federica Ruta and Chiara Esposito for the experimental work performed during their Master's Degree.

Conflicts of Interest: The authors declare no conflict of interest.

References

1. International Energy Agency. *Global CO_2 Emissions Rebounded to Their Highest Level in History in 2021*; International Energy Agency: Paris, France, 2022. Available online: www.iea.org (accessed on 1 March 2022).
2. US Environmental Protection Agency. Overview of Greenhouse Gases. Available online: https://www.epa.gov/ghgemissions/overview-greenhouse-gases (accessed on 1 March 2022).
3. Raza, A.; Gholami, R.; Rezaee, R.; Rezaee, R.; Rasouli, V.; Rabiei, M. Significant aspects of carbon capture and storage—A review. *Petroleum* **2019**, *5*, 335–340. [CrossRef]
4. Erdiwansyah; Mahidin; Husin, H.; Zaki, M. A critical review of the integration of renewable energy sources with various technologies. *Prot. Control Mod. Power Syst.* **2021**, *6*, 1–18. [CrossRef]
5. Tan, H.; Li, J.; He, M.; Li, J.; Zhi, D.; Qin, F.; Zhang, C. Global evolution of research on green energy and environmental technologies: A bibliometric study. *J. Environ. Manag.* **2021**, *297*, 113382. [CrossRef] [PubMed]
6. Ozturk, M.; Dincer, I. A comprehensive review on power-to-gas with hydrogen options for cleaner applications. *Int. J. Hydrogen Energy* **2021**, *46*, 31511–31522. [CrossRef]
7. Martínez, J.; Hernández, E.; Alfaro, S.; López, M.R.; Valverde, A.G.; Albiter, E.; Valenzuela, M.A. High Selectivity and Stability of Nickel Catalysts for CO_2 Methanation: Support Effects. *Catalysts* **2019**, *9*, 24. [CrossRef]
8. Ahn, J.Y.; Chang, S.W.; Lee, S.M.; Sung, S.K.; Woo, J.C.; Jung, C.L.; Yong, J.C.; Kyung, S.S.; Dea, H.M.; Dinh, D.N. Developing Ni-based honeycomb-type catalysts using different binary oxide-supported species for synergistically enhanced CO_2 methanation activity. *Fuel* **2019**, *250*, 277–284. [CrossRef]
9. Gac, W.; Zawadzki, W.; Słowik, G.; Sienkiewicz, A.; Kieryset, A. Nickel catalysts supported on silica microspheres for CO_2 methanation. *Microporous Mesoporous Mater.* **2018**, *272*, 79–91. [CrossRef]
10. Quindimil, A.; De-La-Torre, U.; Pereda-Ayo, B.; Davó-Quiñonero, A.; Bailón-García, E.; Lozano-Castelló, D.; González-Marcos, J.A.; Bueno-López, A.; González-Velasco, J.R. Effect of metal loading on the CO_2 methanation: A comparison between alumina supported Ni and Ru catalysts. *Catal. Today* **2020**, *356*, 419–432. [CrossRef]
11. López-Rodríguez, S.; Davó-Quiñonero, A.; Bailón-García, E.; Lozano-Castelló, D.; Bueno-López, A. Effect of Ru loading on Ru/CeO_2 catalysts for CO_2 methanation. *Mol. Catal.* **2021**, *515*, 111911. [CrossRef]
12. Porta, A.; Falbo, L.; Visconti, C.G.; Lietti, L.; Bassano, C.; Deiana, P. Synthesis of Ru-Based catalysts for CO_2 methanation and experimental assessment of intraporous transport limitations. *Catal. Today* **2020**, *343*, 38–47. [CrossRef]
13. Tsiotsias, A.I.; Charisiou, N.D.; Yentekakis, I.V.; Goula, M.A. Bimetallic Ni-Based Catalysts for CO_2 Methanation: A Review. *Nanomaterials* **2021**, *11*, 28. [CrossRef] [PubMed]
14. Botzolaki, G.; Goula, G.; Rontogianni, A.; Nikolaraki, E.; Chalmpes, N.; Zygouri, P.; Karakassides, M.; Gournis, D.; Charisiou, N.; Goula, M.; et al. CO_2 Methanation on Supported Rh Nanoparticles: The combined Effect of Support Oxygen Storage Capacity and Rh Particle Size. *Catalysts* **2020**, *10*, 944. [CrossRef]
15. Martin, N.M.; Hemmingsson, F.; Wang, X.; Merte, L.R.; Hejral, U.; Gustafson, J.; Skoglundh, M.; Meira, D.M.; Dippel, A.; Gutowski, O.; et al. Structure–Function relationship during CO_2 methanation over Rh/Al_2O_3 and Rh/SiO_2 catalysts under atmospheric pressure conditions. *Catal. Sci. Technol.* **2018**, *8*, 2686–2696. [CrossRef]
16. Martin, N.M.; Hemmingsson, F.; Schaefer, A.; Ek, M.; Merte, L.R.; Hejral, U.; Gustafson, J.; Skoglundh, M.; Dippel, A.; Gutowski, O. Structure-Function relationship for CO_2 methanation over ceria supported Rh and Ni catalysts under atmospheric pressure conditions. *Catal. Sci. Technol.* **2019**, *9*, 1644–1653. [CrossRef]
17. Arandiyan, H.; Kani, K.; Wang, Y.; Jiang, B.; Kim, J.; Yoshino, M.; Rezaei, M.; Rowan, A.E.; Dai, H.; Yamauchi, Y. Highly selective reduction of carbon dioxide to methane on novel mesoporous Rh catalysts. *ACS Appl. Mater. Interfaces* **2018**, *10*, 24963–24968. [CrossRef] [PubMed]

18. Palma, V.; Cortese, M.; Renda, S.; Ruocco, C.; Martino, M.; Meloni, M.E. A Review about the Recent Advances in Selected NonThermal Plasma Assisted Solid–Gas Phase Chemical Processes. *Nanomaterials* **2020**, *10*, 1596. [CrossRef]
19. Wang, B.; Mikhail, M.; Galvez, M.E.; Cavadias, S.; Tatoulian, M.; Costa, P.D.; Ognier, S. Coupling experiment and simulation analysis to investigate physical parameters of CO_2 methanation in a plasma-Catalytic hybrid process. *Plasma Process. Polym.* **2020**, *17*, 1900261. [CrossRef]
20. Feng, X.; Liu, H.; He, C.; Shen, Z.; Wang, T. Synergistic effects and mechanism of a non-Thermal plasma catalysis system in volatile organic compound removal: A review. *Catal. Sci. Technol.* **2018**, *8*, 936–954. [CrossRef]
21. Dębek, R.; Azzolina-Jury, F.; Travert, A.; Maugé, F. A review on plasma-Catalytic methanation of carbon dioxide—Looking for an efficient catalyst. *Renew. Sustain. Energy Rev.* **2019**, *116*, 109427. [CrossRef]
22. Bogaerts, A.; Neyts, E.C. Plasma Technology: An Emerging Technology for Energy Storage. *ACS Energy Lett.* **2018**, *3*, 1013–1027. [CrossRef]
23. Da Costa, P.; Hasrack, G.; Bonnety, J.; Henriques, C. Ni-Based catalysts for plasma-assisted CO_2 methanation. *Curr. Opin. Green Sustain. Chem.* **2021**, *32*, 100540. [CrossRef]
24. Biset-Peiró, M.; Guilera, J.; Zhang, T.; Arbiol, J.; Andreu, T. On the role of ceria in Ni-Al_2O_3 catalyst for CO_2 plasma methanation. *Appl. Catal. A Gen.* **2019**, *575*, 223–229. [CrossRef]
25. Xu, S.; Chansai, S.; Shao, Y.; Xu, S.; Wang, Y.; Haigh, S.; Mu, Y.; Jiao, Y.; Stere, C.E.; Chen, H.; et al. Mechanistic study of non-thermal plasma assisted CO_2 hydrogenation over Ru supported on MgAl layered double hydroxide. *Appl. Catal. B Environ.* **2020**, *268*, 118752. [CrossRef]
26. Nizio, M.; Albarazi, A.; Cavadias, S.; Amouroux, J.; Galvez, M.E.; Da Costa, P. Hybrid plasma-catalytic methanation of CO_2 at low temperature over ceria zirconia supported Ni catalysts. *Int. J. Hydrogen Energy* **2016**, *41*, 11584–11592. [CrossRef]
27. Nizio, M.; Benrabbah, R.; Krzak, M.; Debek, R.; Motak, M.; Cavadias, S.; Gálvez, M.E.; Da Costa, P. Low temperature hybrid plasma-Catalytic methanation over Ni-Ce-Zr hydrotalcite-derived catalysts. *Catal. Commun.* **2016**, *83*, 14–17. [CrossRef]
28. Xu, W.; Dong, M.; Di, L.; Zhang, X. A Facile Method for Preparing UiO-66 Encapsulated Ru Catalyst and its Application in Plasma-Assisted CO_2 Methanation. *Nanomaterials* **2019**, *9*, 1432. [CrossRef]
29. Weng, W.; Pei, X.; Li, J.; Luo, C.; Liu, Y.; Lin, H.; Huang, C.; Wan, H. Effects of calcination temperatures on the catalytic performance of Rh/Al_2O_3 for methane partial oxidation to synthesis gas. *Catal. Today* **2006**, *117*, 53–61. [CrossRef]
30. Mazzieri, V.; Coloma-Pascual, F.; Arcoya, A.; L'Argentière, P.C.; Fıgoli, N.S. XPS, FTIR and TPR characterization of Ru/Al_2O_3 catalysts. *Appl. Surf. Sci.* **2003**, *210*, 222–230. [CrossRef]
31. Benrabbah, R.; Cavaniol, C.; Liu, H.; Ognier, S.; Cavadias, S.; Gálvez, M.E.; Da Costa, P. Plasma DBD activated ceria-Zirconia-Promoted Ni-Catalysts for plasma catalytic CO_2 hydrogenation at low temperature. *Catal. Commun.* **2016**, *89*, 73–76.
32. Zeng, Y.; Tu, X. Plasma-Catalytic CO_2 hydrogenation at low temperatures. *IEEE Trans. Plasma Sci.* **2016**, *44*, 405–411. [CrossRef]
33. Zeng, Y.; Tu, X. Plasma-Catalytic hydrogenation of CO_2 for the cogeneration of CO and CH_4 in a dielectric barrier discharge reactor: Effect of argon addition. *J. Phys. Appl. Phys.* **2017**, *50*, 184004. [CrossRef]
34. Lee, C.J.; Lee, D.H.; Kim, T. Enhancement of methanation of carbon dioxide using dielectric barrier discharge on a Ruthenium catalyst at atmospheric conditions. *Catal. Today* **2017**, *293*, 97–104. [CrossRef]